

**DSCC2014-6033**

**EMPIRICAL MODIFICATIONS TO A PHASE SPACE PLANNER WHICH  
COMPENSATES FOR LOW STIFFNESS ACTUATION IN A PLANAR, POINT-FOOT,  
BIPED ROBOT**

**Donghyun Kim**

Human Centered Robotics Laboratory  
Department of Mechanical Engineering  
University of Texas at Austin  
Austin, Texas 78712  
Email: dk6587@utexas.edu

**Ye Zhao**

Mechanical Engineering  
University of Texas at Austin  
Austin, TX, 78712  
yezhao@utexas.edu

**Gray Thomas**

Human Centered Robotics Laboratory  
Department of Mechanical Engineering  
University of Texas at Austin  
Austin, Texas 78712  
Email: gray.c.thomas@gmail.com

**Luis Sentis**

Human Centered Robotics Laboratory  
Department of Mechanical Engineering  
University of Texas at Austin  
Austin, Texas 78712  
Email: lsentis@austin.utexas.edu

**ABSTRACT**

*This paper presents an extensive experimental study of the first steps of the Hume robot. Hume is an adult sized, 20 kg, series-elastic, point-foot biped robot capable of very fast leg movements. In this study, Hume is constrained to planar motion by a linkage mechanism. We present our application of phase space planning to one, two, and three step walking, the last one over an obstacle. In the implementation, we modified the original theory and added ad-hoc adjustments since the robot could not follow the original theory's planned walking trajectories despite their theoretical stability. We present a good correlation between the phase space plans and our various experiments, and an analysis of the robot's final behavior. Overall the planner and ad-hoc modifications allowed us to execute very smooth gaits even over non-flat surfaces but at the same time demonstrated the shortcomings of open loop techniques.*

**1 INTRODUCTION**

Motivated by the struggle to bring humanoid robots out of the laboratory and into direct contact with humans in cluttered and uncertain environments, both indoors and outdoors, we have decided to focus on the difficult problem of dynamic point-foot locomotion, which has been extensively explored yet remains a challenging topic [1, 2, 3, 4, 5, 6, 7, 8]. We designed our robot with point feet in order to lower the complexity of the mechanical system and allow for hyper-agile behavior by minimizing the inertia of the swing leg. Our robot is designed to have high speed, high agility, and moderate efficiency relative to other dynamic walking robots.

Extensive efforts have been put into feedback control strategies [4, 5]. Many attempts have been made to design control systems for walking robots which avoid the use of the most complex, but most accurate, models. Very early studies used feedback control to tie the walking motion to stable limit cycles of the well-understood stable oscillator system [9]. Compass gait robots

with simple sensory feedback were made to traverse unknown rough terrain.[6] Another highly successful control strategy for simple but highly dynamic hopping behavior was to use separate simple controllers for each of the forward running velocity, hopping height, and body attitude.[10] A similarly simple strategy was latter successfully applied to biped walking robots with point feet under a Virtual Model Control (VMC) framework.[2] Using physically intuitive virtual springs and dampers, this approach was used to stabilize Spring Turkey and Spring Flamingo, which are two planar robots with series elastic actuation.

On the other end of the model complexity spectrum, numerous advances in model-based control using rigid body dynamics have achieved high tracking performance at the cost of computational efficiency [4, 1]. Rabbit [8] employs event-based control of the average walking rate by using virtual constraints synchronized with impact dynamics. However, because of the actuator limitations and lack of leg compliance, Rabbit's running is somewhat limited. This led to the design of the new planer biped, MABEL, which has springs in its drivetrain. MABEL [4] successfully performs stable and fast running through a time-invariant feedback control law, virtual constraints, and hybrid zero dynamics. Most of the work above is limited to 2D planar motions. However, the recent development of the ATRIAS robot [1] has begun the transition of point foot bipeds out of their planar constraint mechanisms and into the world of three-dimensional flat terrain walking.

Although a closed-loop control system is preferable, it is not always available for various reasons-e.g., time delay between high-level and low-level controls. In this case, open-loop control is another candidate strategy that is straightforward to implement. By properly tuning predefined actuator commands, this strategy enables bipedal robots to achieve extremely dynamic motions such as sprinting [3] and running flips [11].

In our study, we also eschewed high-level feedback control and relied more heavily on a motion planner based on inverted pendulum dynamics. The inverted pendulum is a simplified model used to abstract complex biped or humanoid dynamics [12, 13, 14]. Zero Moment Point (ZMP), [15, 14, 16], the mainstream planning method which also uses the inverted pendulum model, is designed to manipulate the center of mass (COM) of a full humanoid in order to avoid tipping the foot onto one of its edges. Capture point based methods (CP) [17] take advantage of first-order dynamics within the analytic solution of the inverted pendulum problem to efficiently predict COM behavior given the center of pressure location.

Our planning strategy, which we named phase space planning, avoids use of analytic solutions and thus can handle arbitrary height surfaces [18, 19]. The algorithm, which we proposed in [19], determines when a walking biped should switch feet when the COM is known to be maintaining a height defined by an arbitrary continuous surface. The use of an arbitrary continuous surface is an improvement over methods which assume a

flat height surface and is better suited to rough terrain locomotion and natural walking with slight height variations throughout the stride. In essence, it uses numerical integration of the inverted pendulum model constrained to a somewhat arbitrary continuous height surface. Numerically computing the intersection of two phase space paths corresponds to associating the time frames of two steps. Phase space planning explains the dynamic limitations of dual support using limiting single-support cases and can predict the maximum and minimum acceleration for any point in dual contact.

Although we successfully tackled the problem of path generation for stable walking in our previous study on the planner, a number of limitations (e.g., inaccurate model, impulse from landing, poor position control) prevented its implementation in a real system. In this paper, we present additional methods to address the real system dynamics that do not correlate well with the simple dynamic model of our planner. First, we modified the equation of an inverted pendulum dynamics to consider the influence of a slider linkage. Second, we modified the height surface to smoothly decrease during a landing motion to alleviate the swing foot landing impulse. Third, the COM velocity was boosted at the lifting time to ensure that each step began smoothly.

## 2 Description of Robot System

In this section, we describe the Hume system specifications, the planar constraint mechanism, and our control strategy for experimental implementations.

### 2.1 Bipedal Robot with Series Elastic Actuators

Hume is a human-sized biped robot with series elastic actuators. Series elastic actuators (SEA) [20] use an elastic element to provide lower instantaneous stiffness, external shock absorption, force sensing, and energy storage. These characteristics are desirable specially in the field of legged robots [21, 1, 2, 4]. Hume has a separate SEA for each of its actuated joints. Instead of energy storage, Hume mainly uses its SEA to achieve high bandwidth of force sensing by encoder-based measurement [22]. Each leg has three degrees of freedom (DOF) and the actuators are located as near to the center of the torso as possible. This design principle enables Hume to provide a light and low inertia leg which allows faster swing motions for the same actuator torque limitations. A planar constraint mechanism which prevents torso roll, yaw, and lateral motion is employed to simplify the problem of walking. It consists of two parallel rails with the length of the robot's range walking motion. For planar motions, only 2 DOF (hip and knee flexion/extension) of each leg are controlled to perform sagittal plane walking tasks. Note that a slider linkage modifies the real inverted pendulum dynamics, which will be discussed in detail later in the paper.

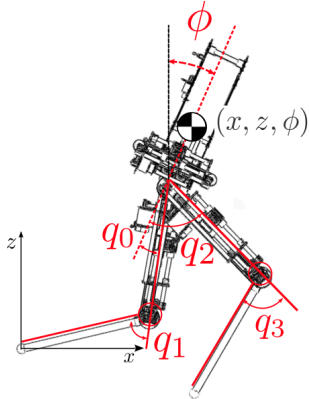


**FIGURE 1.** Hume robot and joint configuration. Each leg of Hume has three actuated joints. For planar motion, only the hip and knee flexion/extension joints are involved in the inverse kinematics. Hip abduction/adduction joints are position controlled to keep the legs in plane. We use a local coordinate system attached to the stance foot contact point.

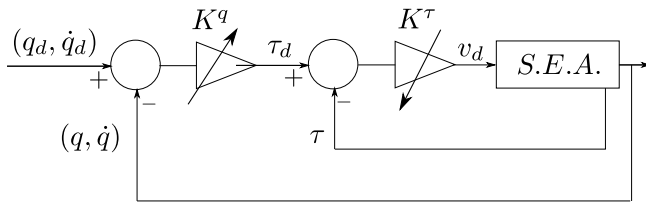


**FIGURE 2.** Cascaded control structure. There are two cascaded feedback loops. The inner loop is a torque feedback loop at the low level. The outer loop is the a joint feedback loop at M3 server level. Both of these two feedback loops are based on PD control.

## 2.2 Open Loop Control

Although the studies about single series elastic actuator proved that accurate and stable control of SEAs is possible[23], achieving accurate position tracking for legged robots with series elastic actuators (SEAs) remains as an open question. The compliant element in SEAs make robot legs quite "soft" and induces sagging errors due to gravity. This problem is usually solved using integral control gains, but we avoided use of integral control since it is known to complicate the stability of the whole robot system. Using high controller gains helps to reduce this gravity-induced error to some degree. However, if the delay between state sensing and controller command is larger than around 1ms, it dramatically degrades the performance of force feedback and can even cause the system to become unstable. The high level control system on our robot has been unable to reduce this delay below 7ms thus far, but the distributed low level system has a 1ms delay. To avoid this latency problem, feedback loops are not adopted in our high level controllers. Instead, we rely on

increasing joint position feedback PD gains  $K_q$  while reducing joint torque feedback PD gains  $K_\tau$  in the distributed system as shown in Fig. 2. The controller gains are manually tuned. This study aims to implement a modified phase space planner with an open loop control strategy at the high level and this simple, joint level feedback strategy at the low level.

## 2.3 Inverse Kinematics

In order to generate joint trajectories at the high level, we employed inverse kinematics based on a known foot location and a planned center of mass location. As will be explained, the center of mass location for this calculation was empirically modified to somewhat offset the effect of the joint sagging in the low level controller. Our inverse kinematics were solved analytically as follows. The cartesian space position vector is defined as  $X = (x_{com}, z_{com}, x_{foot_{sw}}, z_{foot_{sw}}, \phi)^T$ , where  $(x_{com}, z_{com})$  are the horizontal and vertical center of mass (COM) positions,  $(x_{foot_{sw}}, z_{foot_{sw}})$  are the horizontal and vertical swing foot positions, and  $\phi$  is the torso orientation with respect to vertical. The configuration vector in joint space is defined as  $Q = (q_0, q_1, q_2, q_3, \phi)^T$ , where  $(q_0, q_1)$  are the stance leg knee and hip joints respectively and  $(q_2, q_3)$  are the swing leg knee and hip joints respectively (Fig. 1). Here the COM positions  $(x_{com}, z_{com})$  are defined in a local coordinate with the origin at the stance foot  $(x_{foot_{st}}, z_{foot_{st}}) = (0, 0)$ . Then, we derive the following inverse kinematic equations.

$$q_0 = \sin^{-1} \left( \frac{L_1^2 - L_2^2 + x_{com}^2 + z_{com}^2}{2L_1 \sqrt{x_{com}^2 + z_{com}^2}} \right) - \tan^{-1} \left( \frac{x_{com}}{z_{com}} \right) - q_1 + \phi - \frac{\pi}{2} \quad (1)$$

$$q_1 = -\cos^{-1} \left( \frac{(x_{com}^2 + z_{com}^2 - L_1^2 - L_2^2)}{2L_1 L_2} \right) \quad (2)$$

$$q_2 = \cos^{-1} \left( \frac{a^2 + b^2 + L_2^2 - L_1^2}{2L_2 \sqrt{a^2 + b^2}} \right) + \phi + \tan^{-1} \left( \frac{a}{b} \right) \quad (3)$$

$$q_3 = \cos^{-1} \left( \frac{a^2 + b^2 - L_1^2 - L_2^2}{2l_1 l_2} \right) + 2\phi - 2q_2 \quad (4)$$

Where  $a = x_{foot_{sw}} - x_{com}$ ,  $b = z_{com} - z_{foot_{sw}}$  for notational convenience.

## 3 Planner Implementation

The phase space planner we used to accomplish walking motion is modeled on the one proposed in [19]. However, major adjustments were made to compensate for the inaccurate trajectory following of the low level controller and simple inverted pendulum model. Additionally, as previously mentioned, we were unable to implement a high level controller due to stability problems resulting from our large software-induced latency. This

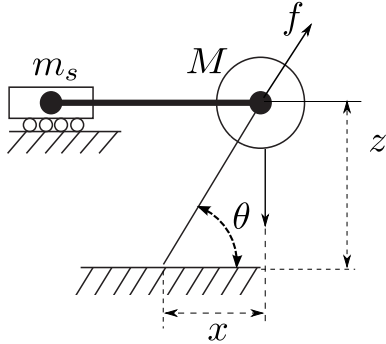


**FIGURE 3. Inverted pendulum with a sliding bar.** The Inverted pendulum model is used to model Hume's dynamics. It has a point foot contact and massless leg. The slider linkage is modeled as an extra mass  $m_s$ , which modifies the pendulum dynamics by a scaling factor. More details refer to Equation (5).

resulted in our use of a joint level position feedback controller which allows the robot to support its weight stably at the cost of high Cartesian position error. In this section, we present three adjustments to our planner which allowed more accurate prediction of the robot's behavior despite these limitations.

### 3.1 Inverted Pendulum with a Sliding Bar

Since we use a slider rocker linkage to keep our robot in plane, the constrained robot system behaves like the articulated bodies of [24] rather than a simpler rigid body as assumed in [19]. The connection between the robot's body and the rocker link, with its constrained slider, means that the combined system does not technically have a center of mass. However, since the rotational joint between the rocker link and the body is very close to the robot's original center of mass, the center of rotation due to an applied force changes only slightly when the direction of the force changes. To keep the model simple we neglect this difference and assume that a center of mass exists. We do, however, model disparate inertia and gravitational forces in the vertical and horizontal directions. With this modification in place we arrive at our updated equation for forward acceleration, following the nomenclature of Fig. 3:

$$\begin{aligned} f \sin \theta &= Mg + M\ddot{z} \\ f \cos \theta &= (M + m_s)\ddot{x} \\ \tan \theta &= \frac{z}{x} \\ \therefore \ddot{x} &= \frac{Mx}{(M + m_s)z}(g + \ddot{z}) \end{aligned} \quad (5)$$

Here  $f$  and  $M$  are the reaction force and robot mass, respectively. As you can see, the ratio  $\frac{M}{M+m_s}$  modifies the familiar dynamic equation of a pendulum constrained to a height surface.

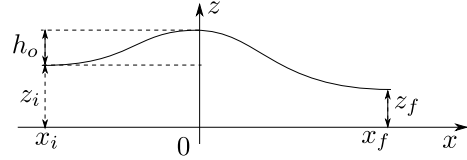


**FIGURE 4. COM path.**

Additionally, while we assume a COM exists, we use an empirically determined estimate for its location. We found this estimate by moving the body towards the forward tipping point in dual support, and iteratively moving the COM estimate towards the line extending vertically from the forward foot at the instant tipping began. This method produced an approximation which is slightly behind our robot manufacturer's COM estimate for the body link.

### 3.2 COM Path Modification to Account for Swing Foot Landing Impulse

One of the advantages of phase space planning is that we can plan for any continuous COM height surface. Knowing that our controller behaves badly in the presence of large impacts, we designed a height surface which reduces the impact of landing. To do this we smoothly reduce the COM height at the end of the stepping motion, resulting in the path shown in Fig. 4. This COM path is composed of two sinusoidal parts, which meet at the peak height with first order continuity. The sinusoidal parts are derived from the height surface parameters. The first part is found

$$\begin{aligned} z &= z_i + \frac{1}{2}h_o(1 - \cos(\frac{x}{-x_i}\pi)) \\ a &= \frac{1}{2}h_o\left(\frac{\pi}{-x_i}\right)\sin(\frac{x-x_i}{-x_i}\pi) \\ b &= \frac{1}{2}h_o\left(\frac{\pi}{x_f}\right)^2\cos(\frac{x-x_i}{-x_i}\pi) \end{aligned} \quad (6)$$

And the second

$$\begin{aligned} z &= z_f + \frac{1}{2}(z_i + h_o - z_f)(1 + \cos(\frac{x}{x_f}\pi)) \\ a &= -\frac{1}{2}(z_i + h_o - z_f)\left(\frac{\pi}{x_f}\right)\sin(\frac{x}{x_f}\pi) \\ b &= -\frac{1}{2}(z_i + h_o - z_f)\left(\frac{\pi}{x_f}\right)^2\cos(\frac{x}{x_f}\pi) \end{aligned} \quad (7)$$

The height path is a function of horizontal position. This is converted to a feed-forward position trajectory by first determining the horizontal position as a function of time. This calculation is performed recursively as a discrete integration. Using

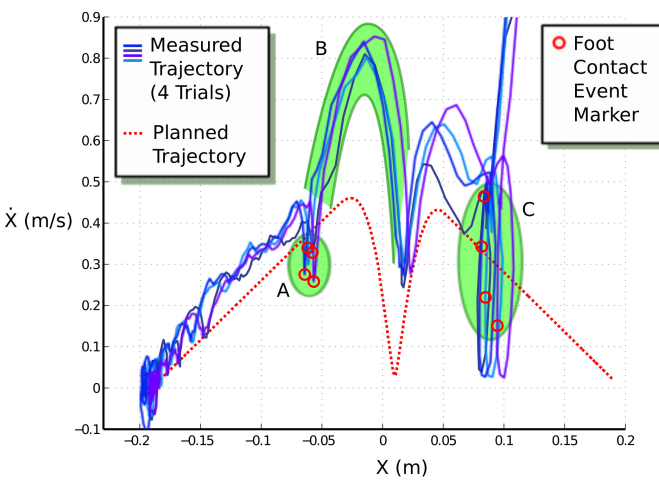


**FIGURE 5. COM trajectories for separate single step experiments without the post-lift-off speed boost.** Swing phase starts in area A, and ends in area C. Area B represents a period of high body tilt rate. At the landing point, there is impact from the ground, and body velocity is dramatically increased. The measured data disobeys the rules of phase space plots to some extent because the joint velocities are filtered before they are used to compute the center of mass velocity and thus it is an imperfect derivative of the center of mass position. Foot contact events in area C immediately follow an extremely high acceleration foot halting motion. Data after landing is omitted, since the forward kinematics do not take into account the observed lifting of the stance foot during impact. The robot rocks considerably after landing.

$R_m = \frac{M}{M+m_s}$  as the ratio of effective masses and  $\Delta t$  as the integration time step, the following equations describe the iteration  $n$  of the integration procedure.

$$A = \frac{x}{z} R_m (g + b \dot{x}^2) \quad (8)$$

$$B = 1 - R_m \frac{x}{z} a \quad (9)$$

$$\dot{x}_{n+1} = \frac{A}{B} \quad (10)$$

$$\ddot{x}_{n+1} = \dot{x}_n + \ddot{x}_n \Delta t \quad (11)$$

$$x_{n+1} = x_n + \dot{x}_n \Delta t + 0.5 \ddot{x}_n \Delta t^2 \quad (12)$$

Here,  $a, b$  are the values defined in the previous equation 6,7.

### 3.3 Post-Lift-Off Speed Boost

We experimentally found that after lifting the stance foot, the phase space data displayed an unexpected acceleration when we successfully initiated a step. Fig. 5 shows this acceleration in

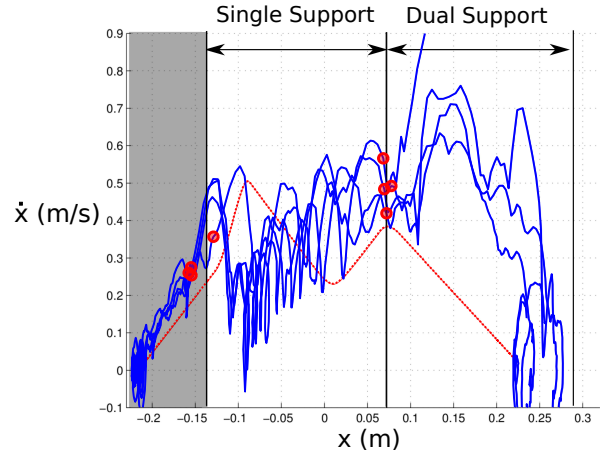


**FIGURE 6. COM x Phase Space Path of Single Step Test.** The red line indicates the planned path and the blue lines represent three separate trials. The red circles indicate the time when the foot is left and landed. The shaded area highlights the initial dual support phase. After lifting the foot, the robot follows inverted pendulum dynamics. After foot touchdown, the COM velocity smoothly decreases.

area B. Later analysis showed this acceleration to be correlated with angular acceleration of the body. As originally designed, the planner creates trajectory based on a constant body pitch, however in our experimental setup the pitch deviates considerably from our intended pitch, and it helps to boost body velocity. In a similar study, Jerry Pratt slightly perturbed the robot with a push to initiate step motion[2]. In our case, the speed boost which is presented by a sinusoidal segment in phase space is inserted into the phase space plan at the point of foot liftoff. As a temporary, ad-hoc method of computing this boost, the post boost phase space path is literally the second part of the original phase space path translated in both velocity and position.

## 4 Experiment

In this paper we performed three types of experiments on the Hume robot: single step, double step, and triple step with an obstacle. In the first two types the floor is flat and level.

### 4.1 Single Step

In this experiment, the motion consists of three parts - dual support forward acceleration of the body, a quick swing leg motion during single support, and a steady deceleration after landing (Fig. 8).

As can be seen in Fig.6, the planned COM path has been modified to include the lift-off speed boost and the real data demonstrates a very similar behavior when the single support phase starts. With this boost we allow the robot to move more closely

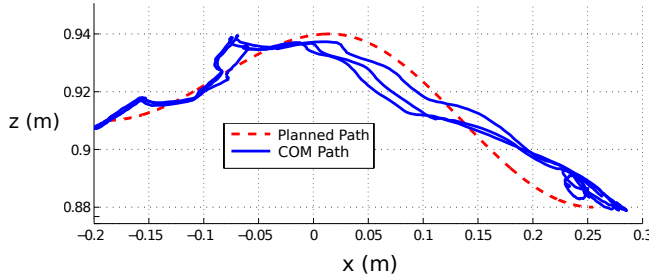


**FIGURE 7.** COM height surface tracking in the xz-plane. The red line indicates the desired surface, and the blue the experimental height surface of the three trials.

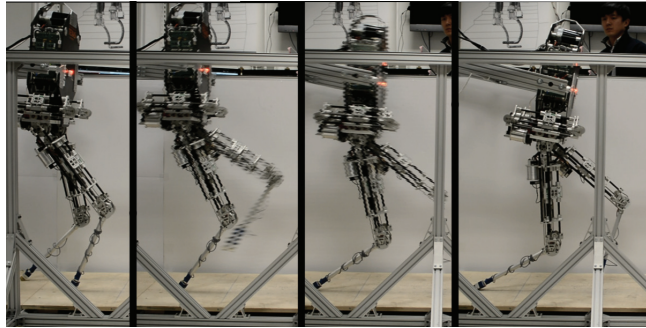


**FIGURE 8.** One step test. Images progress from left to right.

follow inverted pendulum dynamics in single support, compensating for the sudden tilting caused by the unmodeled motion of swing leg at lifting time. At the end of single support, the swing foot lands very close to the intended time determined by the planner. Given our simple planner, the impact occurring due to foot touchdown is not avoided, and causes a rotation of the body. This causes the high COM velocity seen after landing in the phase space. Despite this rotation effect, the overall motion is smooth and the COM path converges to zero velocity with slight torso rotation continuing to be highly visible in the phase space. Fig. 7 shows the COM height surface tracking, with the planned reduction in height being ultimately achieved. One of the most important reasons why the phase space of the forward COM position is similar to the plan is the relatively accurate tracking of this height surface.

Another important point which we have to be careful about is the velocity of the swing leg. When the velocity of a swing leg is too large, the dynamics of the swing leg, which are not considered in the inverted pendulum model, cannot be ignored. Empirically, so far as hip joint velocity remains below 5 rad/s (Fig. 9) with knee joint velocity below 10 rad/s, the robot deviates acceptably little from inverted pendulum dynamics.

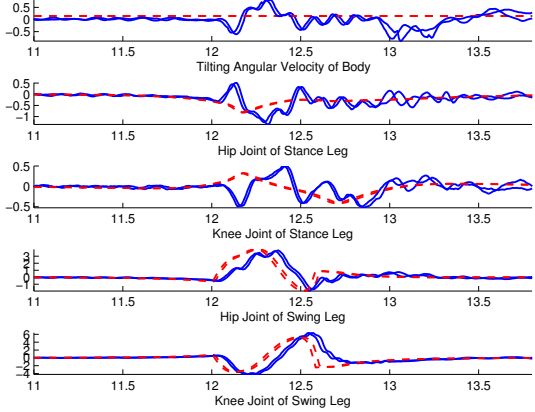


**FIGURE 9.** Angular velocity of the body and the joints during the one step test. x-axis is time (sec) and y-axis is angular velocity (rad/sec). The red dotted lines presents planned velocity trajectories and blue lines are experimental data from two trials. The angular velocity of the hip joint and the knee joint of the swing leg is bounded within 5 rad/s and 10 rad/s during motion, respectively.

#### 4.2 Double Step

In the one step test, we show that our techniques are capable of handling our real robot dynamics. However the walking is simplified by the dual contact at the end. With this result, we attempted to make robot not only step but also walk. The results are shown in Fig. 12 and show that actual behavior is similar to the planned trajectory even though there is velocity noise caused by wobbling motions.

#### 4.3 Three Steps on non-flat surface

Since our ultimate goal is making Hume walk on rough terrain, it is important to see whether Hume can step on and off of small obstacles. In this experiment, an 8cm tall wooden block is used as an obstacle and its position is known a priori by the planner. Snapshots of this experiment are presented in the Fig. 11. The emergency support cable remained slack throughout the motion.

### 5 Conclusion

This experiment demonstrates Hume's ability to achieve smooth walking trajectories and confirms the viability of using open loop planning in planar robots with point feet. It is clear, however, that 3D bipedal walking with point feet will not be possible without a high level feedback controller. We have found that it is advantageous to use SEAs since they deal well with the impulse of landing. We conclude that using SEAs has both been a huge challenge and a huge aid to Hume's performance.

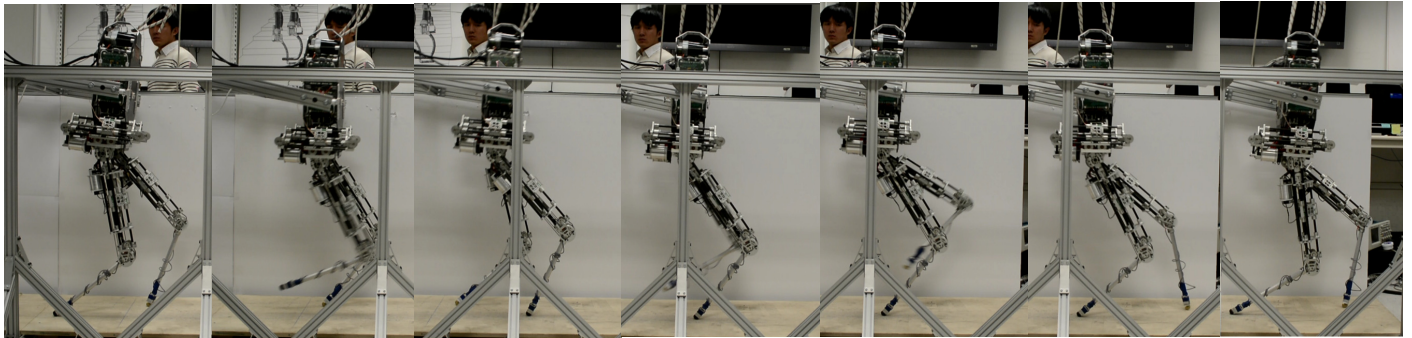


**FIGURE 10.** Two step walk. This video shows the side view of Hume's two step walk.

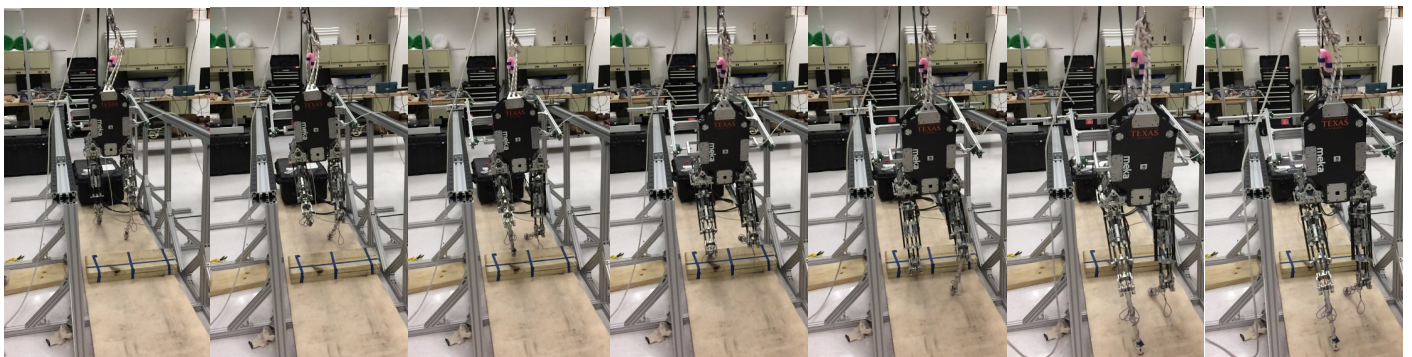


**FIGURE 11.** Three step walk over an obstacle. Hume successfully takes three steps and surmounts an obstacle. Here the planner is fully aware of the obstacle a priori.

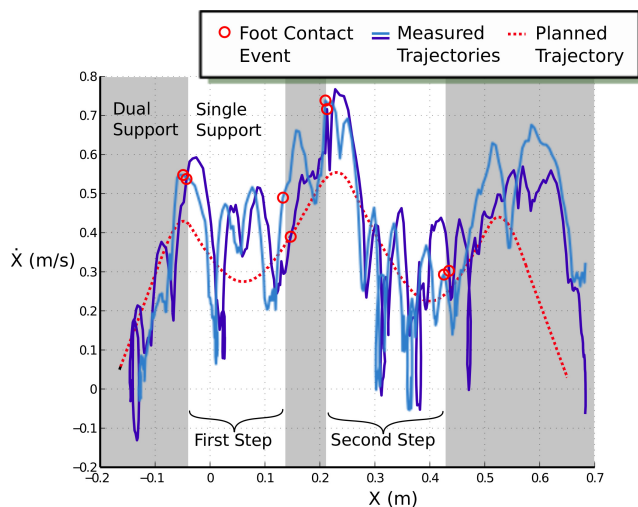


**FIGURE 12.** Phase space for COM  $x$  in the two step test. There is a small dual contact region between steps to improve stability.

In particular, achieving high stiffness which can reject gravity is a challenging task. On the other hand having SEAs allowed us to experiment with high impact forces in a repetitive manner

without damaging the mechanical structure of the robot. Overall the lessons that this study brings to our team are very valuable, both at the hardware and the control levels, to our ultimate goal of unconstrained locomotion over rough terrain using feedback control and inverse dynamics.

## REFERENCES

- [1] Ramezani, A., Hurst, J. W., Hamed, K. A., and Grizzle, J., 2012. "Performance analysis and feedback control of atrias, a 3d bipedal robot". *Journal of Dynamic Systems, Measurement, and Control, under review*.
- [2] Pratt, J., 2001. "Virtual Model Control: An Intuitive Approach for Bipedal Locomotion". *The International Journal of Robotics Research*, **20**(2), Feb., pp. 129–143.
- [3] Niiyama, R., Nishikawa, S., and Kuniyoshi, Y., 2012. "Biomechanical approach to open-loop bipedal running with a musculoskeletal athlete robot". *Advanced Robotics*, **26**(3-4), pp. 383–398.
- [4] Sreenath, K., Park, H.-W., Poulakakis, I., and Grizzle, J., 2013. "Embedding active force control within the compliant hybrid zero dynamics to achieve stable, fast running on mabel". *The International Journal of Robotics Research*,

- 32(3), pp. 324–345.
- [5] Kolathaya, S., and Ames, A. D., 2012. “Achieving bipedal locomotion on rough terrain through human-inspired control”. *Safety, Security, and Rescue Robotics, IEEE International Symposium on*.
- [6] Iida, F., and Tedrake, R., 2009. “Minimalistic control of a compass gait robot in rough terrain”. In *Robotics and Automation, 2009. ICRA’09. IEEE International Conference on*, IEEE, pp. 1985–1990.
- [7] Collins, S. H., Wisse, M., and Ruina, A., 2001. “A three-dimensional passive-dynamic walking robot with two legs and knees”. *The International Journal of Robotics Research*, 20(7), pp. 607–615.
- [8] Westervelt, E., Buche, G., and Grizzle, J., 2004. “Experimental validation of a framework for the design of controllers that induce stable walking in planar bipeds”. *The International Journal of Robotics Research*, 23(6), pp. 559–582.
- [9] Katoh, R., and Mori, M., 1984. “Control method of biped locomotion giving asymptotic stability of trajectory”. *Automatica*, 20(4), pp. 405–414.
- [10] Raibert, M. H., et al., 1986. *Legged robots that balance*, Vol. 3. MIT press Cambridge, MA.
- [11] Hodgins, J. K., and Raibert, M. H., 1990. “Biped gymnastics”. *The International Journal of Robotics Research*, 9(2), pp. 115–128.
- [12] Kajita, S., Kanehiro, F., Kaneko, K., Yokoi, K., and Hirukawa, H., 2001. “The 3d linear inverted pendulum mode: A simple modeling for a biped walking pattern generation”. In *Intelligent Robots and Systems, 2001. Proceedings. 2001 IEEE/RSJ International Conference on*, Vol. 1, IEEE, pp. 239–246.
- [13] Takenaka, T., Matsumoto, T., and Yoshiike, T., 2009. “Real time motion generation and control for biped robot-1st report: Walking gait pattern generation”. In *Intelligent Robots and Systems, 2009. IROS 2009. IEEE/RSJ International Conference on*, IEEE, pp. 1084–1091.
- [14] Hirai, K., Hirose, M., Haikawa, Y., and Takenaka, T., 1998. “The development of honda humanoid robot”. In *Robotics and Automation, 1998. Proceedings. 1998 IEEE International Conference on*, Vol. 2, IEEE, pp. 1321–1326.
- [15] Vukobratović, M., and Borovac, B., 2004. “Zero-moment pointthirty five years of its life”. *International Journal of Humanoid Robotics*, 1(01), pp. 157–173.
- [16] Sugihara, T., Nakamura, Y., and Inoue, H., 2002. “Real-time humanoid motion generation through zmp manipulation based on inverted pendulum control”. In *Robotics and Automation, 2002. Proceedings. ICRA’02. IEEE International Conference on*, Vol. 2, IEEE, pp. 1404–1409.
- [17] Koolen, T., De Boer, T., Rebula, J., Goswami, A., and Pratt, J., 2012. “Capturability-based analysis and control of legged locomotion, Part 1: Theory and application to three simple gait models”. *The International Journal of Robotics Research*, 31(9), Aug., pp. 1094–1113.
- [18] Sentis, L., and Slovich, M., 2011. “Motion planning of extreme locomotion maneuvers using multi-contact dynamics and numerical integration”. In *Humanoid Robots (Humanoids), 2011 11th IEEE-RAS International Conference on*, IEEE, pp. 760–767.
- [19] Zhao, Y., and Sentis, L., 2012. “A three dimensional foot placement planner for locomotion in very rough terrains”. In *Humanoid Robots (Humanoids), 2012 12th IEEE-RAS International Conference on*, pp. 726–733.
- [20] Pratt, G. A., and Williamson, M. M., 1995. “Series elastic actuators”. In *Intelligent Robots and Systems 95. ’Human Robot Interaction and Cooperative Robots’, Proceedings. 1995 IEEE/RSJ International Conference on*, pp. 399–406.
- [21] Hutter, M., Remy, C. D., Hoepflinger, M. A., and Siegwart, R., 2011. “Scarleth: Design and control of a planar running robot”. In *Intelligent Robots and Systems (IROS), 2011 IEEE/RSJ International Conference on*, IEEE, pp. 562–567.
- [22] Slovich, M., Paine, N., Kemper, K., Metzger, A., Edsinger, A., Weber, J., and Sentis, L., 2012. “Hume: A bipedal robot for human-centered hyper-agility”.
- [23] Paine, N., Oh, S., and Sentis, L., 2013. “Design and Control Considerations for High-Performance Series Elastic Actuators”. *Mechatronics, IEEE/ASME Transactions on*(99), pp. 1–12.
- [24] Featherstone, R., 2008. *Rigid body dynamics algorithms*, Vol. 49. Springer Berlin.